Electron-phonon interaction in two dimensions: Variation of $\mathrm{Im}\Sigma(\epsilon_p, \omega)$ with increasing ω_D/E_F

Vladimir N. Kostur and Božidar Mitrović
Department of Physics, Brock University, St. Catharines, Ontario, Canada L2S 3A1
(Received 22 July 1993)

The interaction between phonons and a two-dimensional (2D) electron gas is studied beyond the Migdal approximation. The analysis of the vertex function leads to the relative correction of $|\mathrm{Im}\Sigma(\epsilon_p, \omega)|$ which is of the order of $\lambda(\Omega_{\mathrm{ph}} + aT)E_F^{-1} \ln(E_F/\Omega_{\mathrm{ph}})$. Here, Ω_{ph} is the average phonon frequency, and $a(\sim 1)$ is the ratio between coupling constants for low-frequency and high-frequency phonon modes. For $|\omega| \gg \Omega_{\mathrm{ph}}$, the correction is $|\omega|/E_F$. The physically relevant result is that significant corrections are present only when $|\omega| \lesssim \Omega_{\mathrm{ph}}, |\omega - \epsilon_p| \lesssim \Omega_{\mathrm{ph}}$ and they increase with temperature as T^δ with $\delta \leq 1$ in the entire frequency region. Also, our results strongly suggest that the quasiparticle picture for a 2D electron gas in a 3D lattice has to be corrected by many-particle effects even at small ω_D/E_F.

I. INTRODUCTION

The photoemission studies of high-T_c Cu-O superconductors[1,2] have reported the observation of the effective Fermi energy $E_F^* \simeq 0.3 - 0.5$ eV, which is much smaller than in the usual superconductors. At the same time, the neutron scattering experiments[3] have found that the phonon energies in these materials extend up to 80 meV. Some of the superconductive tunneling experiments[4] have been interpreted in terms of the phonon-induced structure in the tunneling density of states and the results have been analyzed within the usual Eliashberg theory.[5] The extracted Eliashberg function $\alpha^2F(\Omega)$ indicates that electrons couple to all the phonons and the reported values of the parameter $\lambda = 2\int_0^{\Omega_{\mathrm{max}}} \alpha^2F(\Omega)/\Omega$ were large. Moreover, results from the far-infrared measurements[6] and Raman spectroscopy[7] give support to the fact that electron-phonon interaction is not weak for optical phonons in the copper-oxide superconductors. The second important feature of Cu-O superconductors is their layered structure as indicated by transport measurement,[8] band structure calculations,[9] etc. All these results suggest that the usual Migdal approximation[10] for electron-phonon interaction has to be reanalyzed in view of the quasi-two dimensionality and a larger than usual value for the ratio Ω_{ph}/E_F (Ω_{ph} is the average phonon frequency). It was pointed out recently by Eliashberg[11] that in two dimensions (2D) Migdal's theorem applies to the accuracy $(\Omega_{\mathrm{ph}}/E_F)\ln(E_F/\Omega_{\mathrm{ph}})$. In this work the frequency (ω), momentum (i.e., ϵ_p) and temperature (T) dependence arising from the vertex corrections in 2D are examined in greater detail. We believe that our results should also apply to any kind of electron-boson interaction in 2D. Many of the theories for copper oxides calculate the electron self-energy due to boson (spin and/or charge fluctuation) exchange without electron-boson three-point vertex Γ (Fig. 1) in spite of the fact that the relevant spectral densities extend over the energy region which is not much smaller than E_F.

We have calculated the lowest-order correction [Fig. 1(a)] and studied the higher-order corrections [Fig. 1(b)] to Migdal's result, $\Sigma^{(M)}(\omega)$, for irreducible electron self-energy. It is found that corrections to $\mathrm{Im}\Sigma^{(M)}(\omega)$ are significant in the region $|\omega| \sim \Omega_{\mathrm{ph}}$ and $|\omega - \epsilon_p| \sim \Omega_{\mathrm{ph}}$. It is necessary to stress that in the case when Ω_{ph}/E_F is larger than its usual value in metals, the electron (and phonon) lines in the vertex correction diagrams have to be dressed by the self-energy effects, since in that case the quasiparticle damping of electrons in intermediate states cannot be ignored. It is shown that the contribution from the $(N+1)$st-order diagram in 2D is of the order $A_N\Omega_{\mathrm{ph}}/E_F$ where A_N is a combinatorical factor. In the region of frequency ω where $\mathrm{Im}\Sigma^{(M)}(\omega)$ is smaller than $\sim \Omega_{\mathrm{ph}}^2/E_F$, the higher-order corrections to the self-energy have the order of magnitude comparable to (or larger than) Migdal's result. In the case of the optical and 2D acoustical phonons, we were able to obtain the analytical form for this result. Also, the electron-phonon problem in 2D is qualitatively

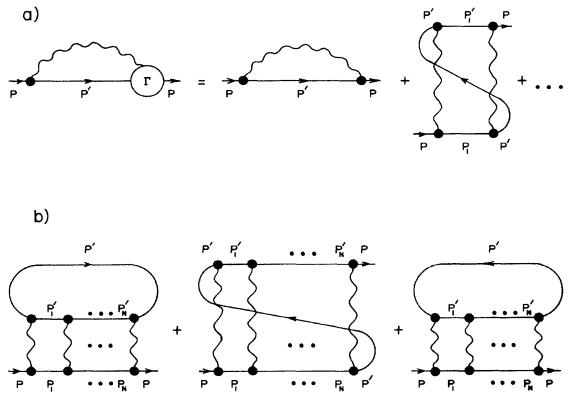

FIG. 1. The skeleton diagrams for the electron self-energy.

0163-1829/93/48(22)/16388(14)/$06.00

different from the same problem in 3D. The immediate difference is in the shape of the phonon density of states $F(\Omega)$ and the Eliashberg function $\alpha^2F(\Omega)$ at small Ω. For example, the Debye model gives $F(\Omega) = 3\Omega^2/\omega_D^3$ and $\alpha^2F(\Omega) = \lambda(\Omega/\omega_D)^2$ in 3D, and $F(\Omega) = 2\Omega/\omega_D^2$ and $\alpha^2F(\Omega) = (\lambda/\pi)\Omega/\sqrt{\omega_D^2 - \Omega^2}$ in 2D. However, the more important effect of reduced dimensionality comes from skeleton diagrams with more than one phonon line.

In Sec. II the second-order correction to self-energy is studied in the case of low-frequency and high-frequency phonon modes. In Sec. III it is shown that a $(N+1)$st-order diagram $(N > 1)$ does not remove this correction. In Sec. IV, the behavior of $\mathrm{Im}\Sigma(\epsilon_p, \omega)$ is analyzed for ω, ϵ_p, and T values on the order of several times Ω_{ph}. Some limiting cases for the three-point vertex are studied in Sec. V. Special attention is paid to changes of $\mathrm{Im}\Gamma$ in 2D. The polarization part at $\mathbf{q} = 0$ is discussed in Sec. VI. The final section contains a summary.

II. THE SECOND-ORDER CORRECTION TO SELF-ENERGY

The electron-phonon interaction is defined by the Frölich Hamiltonian which can be written for a layered structure as

$$H = \sum_{\mathbf{p},i}\left[\epsilon_{\mathbf{p}} c^{\dagger}_{\mathbf{p}i} c_{\mathbf{p}i} + t\sum_{i'=i\pm1} c^{\dagger}_{\mathbf{p}i} c_{\mathbf{p}i'} + \sum_{\mathbf{q}\gamma} g^{(i)}_{\mathbf{q}\gamma} c^{\dagger}_{\mathbf{p}+\mathbf{q}i} c_{\mathbf{p}i}(b^{(i)\dagger}_{\mathbf{q}\gamma} + b^{(i)}_{-\mathbf{q}\gamma})\right] + \sum_{\mathbf{q}\gamma,\mathbf{i}} \Omega^{(i)}_{\mathbf{q}\gamma}(b^{(i)\dagger}_{\mathbf{q}\gamma} b^{(i)}_{\mathbf{q}\gamma} + \tfrac{1}{2}), \tag{1}$$

where instead of the z coordinate the index i is substituted. $\epsilon_{\mathbf{p}}$ is the electron energy, $\Omega^{(i)}_{\mathbf{q}\gamma}$ is the frequency of phonon of polarization γ in the i layer. In the following all the momenta $(\mathbf{p}, \mathbf{q})$ are two dimensional and the momenta in the z direction are defined separately. The hopping matrix element, t, connects only the neighboring layers. Furthermore, we are interested in the limit when t tends to zero. For our purposes it is enough that $t < \Omega^2_{\mathrm{ph}}/E_F$. In our consideration, the ratio between characteristic phonon and electron energies is in the range 0.05–0.2 and a given diagram is computed with the accuracy of $(\Omega_{\mathrm{ph}}/E_F)^2$. Both 2D and 3D phonon dispersions are analyzed.

The Migdal-Eliashberg approach is mainly based on three important assumptions which are in fact interrelated: (1) the dependence of self-energy on $\epsilon_{\mathbf{p}}$ is small; (2) the higher-order vertex corrections are negligible; (3) all the momenta $\mathbf{p}, \mathbf{p}'$ connected to phonon momentum $q = |\mathbf{p} - \mathbf{p}'|$ are on the Fermi surface. The result of Migdal's theorem states, for example, $\mathrm{Im}\Sigma(\epsilon_p, \omega) = \mathrm{Im}\Sigma^{(M)}(\omega) + O(\Omega^2_{\mathrm{ph}}/E_F)$ where

$$\mathrm{Im}\Sigma^{(M)}(\omega) = -\pi\int_0^{\infty} d\Omega\alpha^2F(\Omega)\left[\coth\frac{\Omega}{2T} - \frac{1}{2}\left(\tanh\frac{\Omega+\omega}{2T} + \tanh\frac{\Omega-\omega}{2T}\right)\right] \tag{2}$$

is the imaginary part of the retarded self-energy in the Migdal approximation.

Let us consider the second-order self-energy diagram shown in Fig. 1(a). This diagram is the first from the series of diagrams in the Cooperon channel, and the momentum conservation law $\mathbf{Q} = \mathbf{p} + \mathbf{p}' = \mathbf{p_1} + \mathbf{p}'_1$ is a characteristic of the series. Here $\mathbf{p}$ is the incoming momentum, $\mathbf{p}'$ is the momentum for the electron line crossing the phonon lines, $\mathbf{p_1}$ $(\mathbf{p}'_1)$ is the lower (upper) parallel electron line momentum. The contribution from Nth-order diagram will be denoted by $\Sigma^{(N)}(\epsilon_p, \omega)$. According to Migdal's theorem the vertex Γ [Fig. 1(a)] is equal to the bare vertex g times $[1 + O(\Omega_{\mathrm{ph}}/E_F)]$. Therefore, all the higher-order diagrams give the correction to the self-energy that is of the order of Ω_{ph}/E_F. This implies that if one is to calculate $\Sigma^{(2)}(\epsilon_p, \omega)$ to the accuracy $(\Omega_{\mathrm{ph}}/E_F)^2$, one can substitute in the expression for $\Sigma^{(2)}(\epsilon_p, \omega)$ the dressed functions by the functions calculated within the Migdal-Eliashberg approach [e.g., electron Green's function $G(\epsilon_{p_1}, \omega)$ by $G^{(M)}(\epsilon_{p_1}, \omega)$]. To study the effects of finite E_F, we will consider the spectrum $-\epsilon_p = p^2/2m - \mu$, where μ is the chemical potential, and $E_F = \mu(T = 0)$ is near the top of the band.

The expression for self-energy from the diagram under consideration takes the form[12]

$$\Sigma^{(2)}(\epsilon_p, i\omega_n) = T\sum_{n'} T\sum_{n''}\sum_{\mathbf{p}'\mathbf{p}'_1}\sum_{\gamma',i'} g^{(i')2}_{q_1\gamma'} D^{(i')}_{\gamma'}(q_1, i\omega_{n-n'}) \sum_{\gamma'',i''} g^{(i'')2}_{q_2\gamma''} D^{(i'')}_{\gamma''}(q_2, i\omega_{n-n''})$$
$$\times G(\epsilon_{p_1}, i\omega_{n'}) G(\epsilon_{p'}, i\omega_{n'+n''-n}) G(\epsilon_{p'_1}, i\omega_{n''}). \tag{3}$$

The different thermal factors with the combinations of the real and imaginary parts of the electron and phonon propagators appear after analytical continuations from the Matsubara frequencies to the real axes $i\omega_n \to \omega + i0^+$, $i\omega_{n'} \to \omega'$, $i\omega_{n''} \to \omega''$, and after taking the imaginary part of $\Sigma^{(2)}(\epsilon_p, \omega)$. To eliminate a large number of the integrations which appear after analytical continuation, we convert (when possible) the imaginary parts to the real parts through the dispersion relations. In the final result for $\mathrm{Im}\Sigma^{(2)}(\epsilon_p, \omega)$, there are two integrations over ω', ω'' and two summations over momenta. The expression for $\mathrm{Im}\Sigma^{(2)}(\epsilon_p, \omega)$ can be written as

$$\mathrm{Im}\Sigma^{(2)}(\epsilon_p, \omega) = \sum_{i=0}^{3} S_i(\epsilon_p, \omega). \tag{4}$$

Here $S_0(\epsilon_p,\omega)$ is the term where only the product of the imaginary parts of the phonon and electron Green's functions is included. The sum of the terms involving the product of the imaginary parts of both phonon propagators, two real and one imaginary part of the electron Green's function is denoted as $S_1(\epsilon_p,\omega)$. The sum of the terms containing products of one real and one imaginary part of the phonon propagators and two imaginary parts with a real part of electron propagators is $S_2(\epsilon_p,\omega)$. The product of two real parts of phonon Green's functions and three imaginary parts of electron Green's functions is $S_3(\epsilon_p,\omega)$. All terms $S_i(\epsilon_p,\omega)$ $(i=0,1,2,3)$ contain various thermal factors which are combinations of the Bose and Fermi functions. For example, the expression for S_0 takes the form

$$S_0(\epsilon_p,\omega)=\frac{\pi^3}{4}\int_0^\infty d\Omega_1\int_0^\infty d\Omega_2\sum_{\alpha_1,\alpha_2=\pm1}\left[\coth\frac{\Omega_1}{2T}\coth\frac{\Omega_2}{2T}-\alpha_1\tanh\frac{\omega+\alpha_1\Omega_1}{2T}\right.$$
$$\left.\times\alpha_2\tanh\frac{\omega+\alpha_2\Omega_2}{2T}\right]B^{(2)}(\epsilon_p,\omega;\omega+\alpha_1\Omega_1,\omega+\alpha_1\Omega_1$$
$$+\alpha_2\Omega_2,\omega+\alpha_2\Omega_2;\Omega_1\Omega_2). \tag{5}$$

Here

$$B^{(2)}(\epsilon_p,\omega;\omega',\omega'',\omega''';\Omega_1\Omega_2)=N(0)^{-2}\sum_{\mathbf{p}'\mathbf{p}_1'}B(q_1,\Omega_1)B(q_2,\Omega_2)A(\epsilon_{p_1},\omega')A(\epsilon_{p'},\omega'')A(\epsilon_{p_1'},\omega'''), \tag{6}$$

$$A(\epsilon_p,\omega)=-\frac{1}{\pi}\mathrm{Im}G^R(\epsilon_p,\omega) \tag{7}$$

and $B(q,\Omega)$ is the spectral weight of the phonon propagator

$$\sum_{\gamma,i}g_{q\gamma}^{(i)2}D_\gamma^{(i)}(q,\nu)=N(0)^{-1}\int_0^\infty d\Omega B(q,\Omega)\frac{2\Omega}{(\nu+i0)^2-\Omega^2}, \tag{8}$$

where $N(0)=m/2\pi$ is the density of states at the Fermi level in 2D. The other three functions S_1,S_2,S_3 are also directly related to $B^{(2)}$ (see the Appendix). The dependence of $\mathrm{Im}\Sigma^{(2)}$ on ϵ_p is only through $B^{(2)}$, but the dependence on ω comes from $B^{(2)}$, the thermal factors and, in the case of S_1,S_2,S_3, from the denominators in the spectral representations of propagators.

In 2D the integration over any two of momenta from the set $\mathbf{p_1},\mathbf{p}',\mathbf{p}_1'$ in Eq. (3) [or Eq. (6)] can be replaced by integration over the energy variables $\epsilon_{p_1},\epsilon_{p'},\epsilon_{p_1'}$ and $Q=|\mathbf{p}+\mathbf{p_1}|=|\mathbf{p}'+\mathbf{p}_1'|$. This set of variables is the most natural for the analysis of contribution from the diagrams with more than one phonon line. The Jacobian for transition from the integration over the electron momenta to the integration over the energy variables and Q is defined by the inverse square root from the product of polynomials $X^2(Qpp')X^2(Qp_1p_1')$ where

$$X^2(Qpp')=[Q^2-(p-p')^2][(p+p')^2-Q^2]. \tag{9}$$

This polynomial is biquadratic in each variable and symmetric under the exchange of any pair of variables. This type of polynomial plays a key role not only in $\Sigma^{(2)}$ but also in the higher-order diagrams.[13]

After the change of variables the expression for $B^{(2)}$ takes the form

$$B^{(2)}(\epsilon_p,\omega;\omega',\omega'',\omega''';\Omega_1\Omega_2)=\frac{1}{E_F}\int_{-\infty}^{\mu}d\epsilon_{p_1}A(\epsilon_{p_1},\omega')$$
$$\times\int_{-\infty}^{\mu}d\epsilon_{p'}A(\epsilon_{p'},\omega'')\int_{-\infty}^{\mu}d\epsilon_{p_1'}A(\epsilon_{p_1'},\omega''')\theta(Q_M-Q_m)$$
$$\times\frac{1}{\pi^2}\int_{Q_m}^{Q_M}\frac{(p_F)^2 2QdQ}{X(Qp_1p_1')X(Qpp')}\frac{1}{2}\sum_{\pm}B(q_1^{\pm},\Omega_1)B(q_2^{\mp},\Omega_2). \tag{10}$$

Here $Q_m=\max(|p_1-p_1'|,|p-p'|)$, $Q_M=\min(p_1+p_1',p+p')$, and $\theta(x)$ is the usual step function. The electron momenta are functions of the corresponding energy variables, e.g., $p=p(\epsilon_p)$, etc. The phonon momenta depend on $\epsilon_{p_1},\epsilon_{p'},\epsilon_{p_1'}$ through the electron momenta

$$2q_1^{\pm^2}=p^2+p'^2+p_1^2+p_1'^2-Q^2$$
$$-\frac{1}{Q^2}[(p_1^2-p_1'^2)(p^2-p'^2)$$
$$\pm X(Qp_1p_1')X(Qpp')] \tag{11}$$

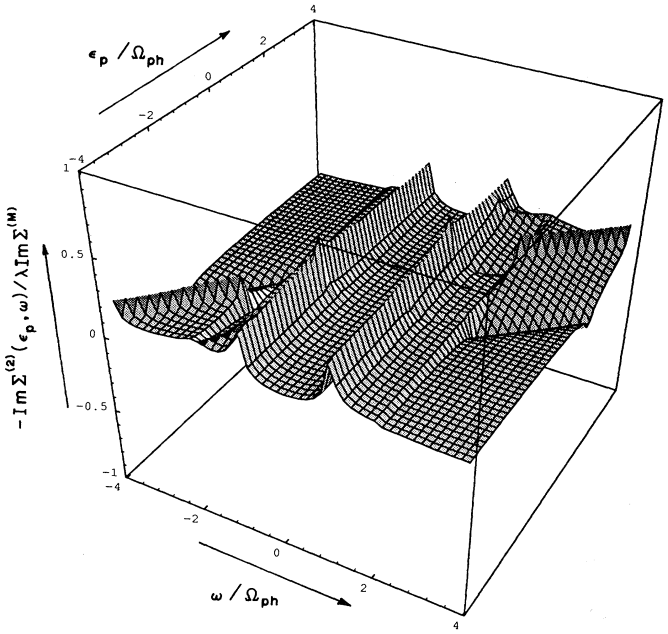

FIG. 2. The correction to the imaginary part of the electron self-energy in 2D for the Einstein model with $\Omega_{\rm ph}^{(0)} = 0.1E_F$ and at $T = 0$. The correction is normalized by the electron-phonon coupling constant, λ, and by $\mathrm{Im}\Sigma^{(M)}(\Omega_{\rm ph}^{(0)} + 0^+)$. The correction is present in the region where Migdal's result is equal to zero.

and $q_2^{\pm}$ can be obtained from (11) by the exchange of p_1 and p_1'. If the electron momenta are near the Fermi surface the derivatives $d\Omega_q/d\epsilon_p$ are of the order of $\Omega_{\rm ph}/E_F$ except when $q \sim 0$, or $Q \sim 0$, or $Q \sim 2p_F$. In order to have one-to-one correspondence between the old and the new variables the integrations over momenta are separated into four sectors. Different signs in (11) correspond to different sectors.

The important feature of Eq. (10) is the presence of E_F^{-1} as a prefactor. We want to estimate $\mathrm{Im}\Sigma^{(2)}(\epsilon_p,\omega)$ for ω and $\epsilon_p \sim \Omega_{\rm ph}$. The order of the magnitude of $\mathrm{Im}\Sigma^{(2)}$ is determined by the function $B^{(2)}$ integrated over the phonon frequencies Ω_1, Ω_2. One finds $\mathrm{Im}\Sigma^{(2)} \sim \lambda^2\Omega_{\rm ph}^2/E_F$ if different factors in the integrand were regular. However, in 2D that is not the case. One can see this by taking the quasiparticle form for the electron spectral weights, $A^{(0)}(\epsilon_p,\omega) = \delta(\omega - \epsilon_p)$. After transforming the integrations over $\mathbf{p}', \mathbf{p}_1'$, Eq. (6), into integrations over $\epsilon_{p_1}, \epsilon_{p'}, \epsilon_{p_1'}$ and Q the integrations over $\epsilon_{p_1}, \epsilon_{p'}, \epsilon_{p_1'}$ in Eq. (10) are trivial and only the integral over momentum Q remains. Note that now the momenta are function ω's: $p_1 = p(\omega')$, $p' = p(\omega'')$, $p_1' = p(\omega''')$. If the square-root singularities from the polynomials (9) coincide, the integral over Q has the logarithmic singularities at the limits of integration Q_m and Q_M. The improper integrals over ω' and ω'', which are present in the expressions for S_1, S_2, and S_3, do not change the type of singularity. Integration over the phonon frequencies Ω_1, Ω_2 does not remove the singularity on the line $\omega = \epsilon_p$ within our accuracy $(\Omega_{\rm ph}/E_F)^2$. A similar kind of singularity has been discussed for Coulomb interaction in 2D.[14] We note, however, that in the higher-order diagrams, the integration over Q produces singularities which are stronger than logarithmic in 2D (see Sec. III). In the following, we will call such type of singularities of the diagrams in 2D geometrical singularities. These geometrical singularities are present in 2D for each diagram if more than one phonon (boson) line appears. This singular behavior could be removed due to the following physical reasons. First, hopping in the z direction leads to a dispersion $-\epsilon_p = p^2/2m - \mu + t\cos(p_z c)$ and additional integration over the z components of momenta gives $\mathrm{Im}\Sigma^{(2)} \sim \lambda^2\Omega_{\rm ph}^2 E_F^{-1}\ln(E_F/t)$.[15] Second, when the diagrams are calculated with the dressed propagators, the damping associated with the imaginary part of self-energy insertions will remove the singular behavior. In the present paper we assume $t \ll \Omega_{\rm ph}$ and therefore consider only the second case.

A. Einstein model for the phonon spectral weight

The result for $\mathrm{Im}\Sigma^{(2)}(\epsilon_p,\omega)/\max|\mathrm{Im}\Sigma^{(M)}|$ calculated with bare electron lines for the Einstein model with a phonon frequency $\Omega_{\rm ph}^{(0)} = 0.1E_F$ and at $T = 0$ is given in Fig. 2. The singularities in $\Sigma^{(2)}$, which were discussed above, have been cut off by taking the difference between arguments near the singularities not smaller than the accuracy of the calculation, i.e., $(\Omega_{\rm ph}^{(0)}/E_F)^2$. We note that at the cutoff near the lines $|\omega| = \Omega_{\rm ph}^{(0)}$ and $|\omega - \epsilon_p| = 0$ the correction due to $\Sigma^{(2)}$ is given by Eliashberg's estimate.[11] An interesting feature of the result shown in Fig. 2 is that corrections are mostly located near the lines $|\omega| = \Omega_{\rm ph}^{(0)}$, $|\omega - \epsilon_p| = 0$, and $|\omega - \epsilon_p| = 2\Omega_{\rm ph}^{(0)}$. More importantly, $\mathrm{Im}\Sigma^{(2)}$ is finite in the region where $\mathrm{Im}\Sigma^{(M)}$ is zero. For the Einstein model $\mathrm{Im}\Sigma^{(M)} = -(\pi/2)\lambda\Omega_{\rm ph}^{(0)}\theta(|\omega| - \Omega_{\rm ph}^{(0)})$ and thus it vanishes for $|\omega| < \Omega_{\rm ph}^{(0)}$. However, at $T = 0$ for $|\omega| < \Omega_{\rm ph}^{(0)}$, $\mathrm{Im}\Sigma^{(2)}$ is equal to S_3, Eq. (4), which is given by

$$S_3 = \frac{\pi}{4}\int_0^{\omega} d\omega' \int_0^{\omega-\omega'} d\omega'' \int_0^{\infty} d\Omega_1 \frac{2\Omega_1}{(\omega'-\omega)^2 - \Omega_1^2} \int_0^{\infty} d\Omega_2 \frac{2\Omega_2}{(\omega''-\omega)^2 - \Omega_2^2} B^{(2)}(\epsilon_p,\omega;\omega',\omega'+\omega''-\omega,\omega'';\Omega_1\Omega_2)\,. \tag{12}$$

B. Coupling to high-frequency modes

In the case of several optical phonon branches the singularities of a simple Einstein model at $|\omega| = \Omega_{\rm ph}^{(0)}$ and $|\omega - \epsilon_p| = 2\Omega_{\rm ph}^{(0)}$ are smeared out, but singularity at $\omega = \epsilon_p$ remains, and the corresponding term in $\mathrm{Im}\Sigma^{(2)}$ is increased due to the presence of several branches. To remove this singularity one has to in-

clude the self-energies in the electron propagators. To the accuracy $(\Omega_{\rm ph}/E_F)^2$, the electron spectral weights in the expression $\Sigma^{(2)}$ can be replaced by $A^{(M)}(\epsilon_p,\omega) = -(1/\pi){\rm Im}\{1/[\omega-\epsilon_p-\Sigma^{(M)}(\omega)]^{-1}\}$ and $B(q,\Omega)$ can be replaced by Migdal's result $\alpha^2F(q,\Omega)$, where[16]

$$\alpha^2F(q,\Omega) = N(0)\sum_{\gamma,i} g_{q\gamma}^{(i)2}\delta(\Omega-\Omega_{q\gamma}^{(i)})\,. \tag{13}$$

The δ function in Eq. (13) appears because of the consequence of Migdal's theorem which states that ${\rm Im}\Pi({\bf q},\Omega) \sim O(\Omega_{\rm ph}^2/E_F)$ except in the small vicinity of $q \sim 0$.[12] Here Π is the polarization part. For high-frequency modes we can ignore the q dependence of $\alpha^2F(q,\Omega)$, and replace this function with the Eliashberg function $\alpha^2F(\Omega)$. The case of low-lying modes with linear phonon dispersion will be studied separately in the next section.

The integration over ϵ_{p_1}, $\epsilon_{p'}$, and $\epsilon_{p_1'}$ in the expression for, say, S_0 [see Eqs. (5) and (10)] can be carried out by using the general result

$$\frac{1}{\pi^3}\int_{-\infty}^{+\infty}\frac{\tau_1^{-1}d\epsilon_1}{\epsilon_1^2+\tau_1^{-2}}\int_{-\infty}^{+\infty}\frac{\tau_2^{-1}d\epsilon_2}{\epsilon_2^2+\tau_2^{-2}}\int_{-\infty}^{+\infty}\frac{\tau_3^{-1}d\epsilon_3}{\epsilon_3^2+\tau_3^{-2}}\ln|\epsilon_1+\epsilon_2+\epsilon_3+\epsilon| = \frac{1}{2}\ln[\epsilon^2+(\tau_1^{-1}+\tau_2^{-1}+\tau_3^{-1})^2]. \tag{14}$$

Here $\epsilon = \epsilon_p - \omega$ and $1/\tau = |{\rm Im}\Sigma^{(M)}|$. For the terms S_i $(i=1,2,3)$ one can use the formula

$$\int_{-1}^{1}\frac{dx}{\sqrt{1-x^2}}\frac{1}{x-z} = \frac{i\pi{\rm sgn}({\rm Im}z)}{\sqrt{1-z^2}} \tag{15}$$

to perform the improper integrations analytically, and then to use a formula analogous to (14). The branch of the square root on the right side of Eq. (15) is such that it has a positive real part. For improper integration it is necessary to substitute real z by $z = z \pm i0$ and to take the real part. It is clear that the logarithmic singularity in each term of the second-order self-energy is removed if at least one τ_i^{-1} is finite. In that case we obtain the result of Ref. 11, if $1/\tau \sim \Omega_{\rm ph}$.

The vicinity of the point $\omega = 0$ represents a special case. If the phonon spectral weight is very small in the region of the low frequencies $[\alpha^2F(\Omega) \simeq 0$ at $\Omega < \Omega_{\rm min}]$ then, due to thermal factors near $T \simeq 0$, ${\rm Im}\Sigma^{(M)}(\omega) \simeq \lambda\Omega_{\rm min}\exp(-\Omega_{\rm min}/T)$ when $\omega < \Omega_{\rm min}$. The terms S_0, S_1, S_2 are exponentially small for the same reasons. It is easy to check that at small ω and at zero temperature the asymptotic value of S_3 is nonzero. We can obtain the estimate for ${\rm Im}\Sigma^{(2)}$ from Eq. (12) in the region of $\omega < \Omega_{\rm min}$: ${\rm Im}\Sigma^{(2)} \simeq (4\pi)^{-1}\lambda^2\omega^2E_F^{-1}\ln(E_F/|\omega-\epsilon_p|)$ at small ω, and $\lambda^2\Omega_{\rm min}^2E_F^{-1}\ln(E_F/\Omega_{\rm min})$ at $\omega \approx \Omega_{\rm min}$. The values are small, but not exponentially small as the term calculated within the Migdal approximation, and the logarithmic singularity is still present due to the absence of damping in this region. To remove the singularity it is necessary to study the low-lying phonon modes more carefully because we cannot ignore the q dependence of the phonon spectral weight in the region of the low frequencies. Nevertheless, we will show in the next section that the main conclusion is the same: the vertex corrections in 2D can be larger than the term calculated within the Migdal approximation in the region of frequencies where the imaginary part of self-energy becomes smaller than about $(\lambda\Omega_{\rm ph})^2/E_F$. The correction is of the order of $\Omega_{\rm ph}/E_F$, and therefore Migdal's statement[10] concerning the size of vertex corrections remains valid.

C. The second-order correction to self-energy at low frequencies

To analyze the behavior of the second-order self-energy in the region of low frequencies we restrict ourselves by studying the case of a phonon branch with the dispersion $\Omega_{q\gamma}^{(i)} = sq < \omega_D$, where s is the sound velocity and ω_D is the Debye frequency. We take $B(q,\Omega)$ to be given by the Migdal approximation: $B(q,\Omega) = \alpha^2F(q,\Omega)$. The numerical calculations of the term $S_0(\epsilon_p,\omega)$ normalized by ${\rm Im}\Sigma^{(M)}$ are shown in Fig. 3 at different temperatures T and quasiparticle energies ϵ_p. The absolute value of the corrections does not exceed $\omega_D^2/E_F\ln(E_F/\omega_D)$,[11] but in the vicinity of $\omega = 0$ they become of the same order as (or even larger than) Migdal's term. Another feature of the results is that the corrections become very flat, do not depend much on ϵ_p at small ω, and increase linearly in the entire region of frequencies at high temperatures (Fig. 3, inset).

We can study ${\rm Im}\Sigma^{(2)}$ analytically for 2D acoustic phonons with bare lines in the vicinity $\omega = 0$ by expansion in the powers of ω_D/E_F. It will be shown that the term S_0 [see Eq. (5)] is a leading term for $\Sigma^{(2)}$ in the vicinity of $\omega = 0$. Since the prefactor in Eq. (10) is

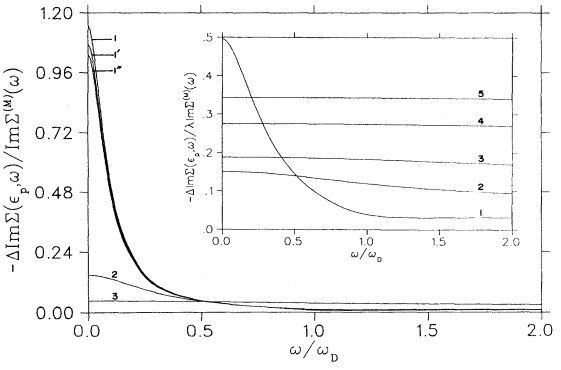

FIG. 3. The temperature dependence of the correction to the imaginary part of the self-energy in 2D from the leading term in ${\rm Im}\Sigma^{(2)}$ (in the vicinity of $\omega = 0$) calculated with spectral weights obtained within the Migdal approximation for Debye model with $\omega_D = 0.05E_F$ and $\lambda = 0.3$. The curves 1, 1′, and 1″ are for $T = 0.03\omega_D$ and $\epsilon_p = 0$, $\epsilon_p = \omega_D$, $\epsilon_p = 2\omega_D$, respectively. Curve 2 corresponds to $T = 0.1\omega_D$, $\epsilon_p = 0$. Curve 3 is for $T = 0.5\omega_D$, $\epsilon_p = 0$. Inset: $\omega_D = 0.05E_F, \lambda = 0.3, \epsilon_p = 0$. Curve 1 is for $T = 0.1\omega_D$, curve 2 is for $T = 0.5\omega_D$, curve 3 is for $T = \omega_D$, curve 4 is for $T = 2\omega_D$, and curve 5 is for $T = 3\omega_D$.

ω_D/E_F one can take into account only the terms of the order of 1, coming from the integration over Q. Furthermore, the imaginary parts of the bare electron Green's functions fix the electron momenta near the Fermi surface with the accuracy ω_D/E_F. Keeping this in mind it is clear that at $T > 0$ S_0 is proportional to T^2 when $q_1 = q_2 = 0$ and $Q = 2p_F$ [Fig. 4(a), case 1], and that it is proportional to T when $q_1 = 0$, $q_2 = q$, and $Q = (2p_F)^2 - q^2$ [Fig. 4(a), case 2] or when $q_1 = 0$, $q_2 = 2p_F$, and $Q = 0$ [Fig. 4(a), case 3]. All phonons are involved in the scattering process at $Q = 0$, but their momenta are correlated by $q_1^2 + q_2^2 = (2p_F)^2$ [Fig. 4(b)]. The processes in Fig. 4(a) (cases 1 and 3) give the logarithmic singularities at $T > 0$:

$$S_0 = \frac{\pi}{4}\lambda^2 \frac{T^2}{E_F}\left[\left(1+\frac{\omega_D}{2T}\coth\frac{\omega_D}{2T}\right)\ln\frac{8E_F}{|\omega-\epsilon_p|} + \frac{\omega_D}{2T}\coth\frac{\omega_D}{2T}\ln\frac{8E_F}{\sqrt{|4\omega_D^2-(\omega-\epsilon_p)^2|}}\right]. \tag{16}$$

Here, $q_D = 2p_F$ is taken for simplicity and the terms without singularities are omited. The logarithmic singularities caused by the geometrical singularities in the case of the acoustic phonons appear only at finite temperature in contrast to the case of high-frequency phonon modes. At $T = 0$ and at $\omega \gg \omega_D^2/E_F$, the processes shown in Fig. 4(b) give the main contribution to S_0 for the bare lines. These processes can be described in the terms of one phonon variable. In this case S_0 can be written in a form completely analogous to $\mathrm{Im}\Sigma^{(M)}$, but with $\alpha^2F(\Omega)$ replaced by an effective spectrum $\alpha^2F_{\mathrm{eff}}(\Omega)$. To obtain this

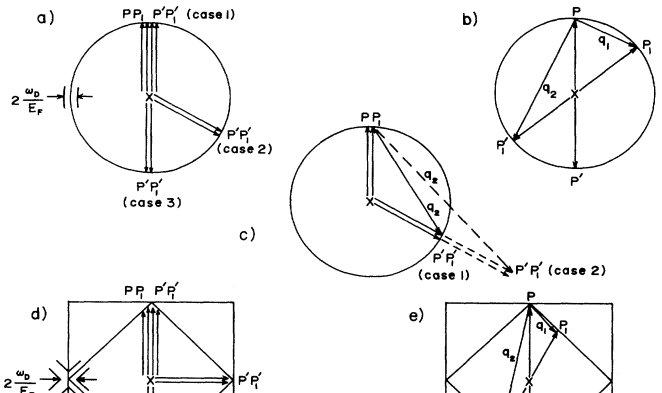

FIG. 4. The special points connected with geometrical singularities in 2D for different shapes of the Fermi surface: (a) and (d) at finite temperatures ($T \neq 0$); (b) and (e) at zero temperature. The difference between electron momenta in each group of parallel lines is $\sim p_F(\omega_D/E_F)$. The scale of $2p_F(\omega_D/E_F)$ at $\omega_D/E_F = 0.1$ is shown for convenience. (c) at $T \simeq \omega \simeq 0$ the processes in the vicinity of the Fermi surface (case 1) give the largest contribution to $\mathrm{Im}\Sigma^{(2)}$ (see the text).

form the integration measure $dQ^2/[X(Qp_1p_1')X(Qpp')]$ is replaced by $\pm 2\mathrm{sgn}[(p_1-p_1')(p-p')]d\theta^{(\pm)}/\sin\theta^{(\pm)}$ in the integral over Q. The signs $\pm$ correspond to the signs in the definition of phonon momenta [see Eq. (11)]. The result is $\alpha^2F_{\mathrm{eff}}(\Omega) = (\pi/4)(\lambda^2\omega_D/4E_F)\omega_D/\sqrt{\omega_D^2-\Omega^2}$. At small ω and T S_0 is given by

$$S_0 = \frac{\pi}{4}\lambda^2\frac{\omega_D}{2E_F}\left[|\omega| + \pi T + T\ln\frac{4E_F}{\sqrt{|\epsilon_p(4\omega_D^2-\epsilon_p^2)|}}\right]. \tag{17}$$

In Eq. (17) we have assumed that $\epsilon_p \sim \omega_D \gg \omega, T$. There are no reasons why this concrete term would be changed by dressing the lines at $T \approx 0$ in the vicinity of $\omega = 0$. Indeed, the calculations with dressed lines (Fig. 3) clearly demonstrate an increase of the correction to $\Sigma^{(M)}$ at small ω and T.

As it was discussed above, at finite temperatures the cutoff of the logarithmic singularity is provided by the finite value of damping. It is well known that $\mathrm{Im}\Sigma^{(M)} \simeq -\pi\lambda T$ at temperatures comparable to ω_D. Therefore, the temperature dependence of $\mathrm{Im}\Sigma^{(2)}$ calculated with dressed lines does not come only from the thermal factors. Upon including the damping, the logarithmic singularity in Eq. (16), which is obtained for bare lines, is replaced by a factor $\sim \ln(E_F/\lambda T)$ and this introduces an additional temperature dependence. At high temperatures, the asymptotic behavior of S_0 for dressed lines can be estimated as $\lambda^2T^2E_F^{-1}\ln(E_F/\lambda T)$. One can conclude that $\mathrm{Im}\Sigma^{(2)}/\mathrm{Im}\Sigma^{(M)}$ is nearly linear in temperature. To find a more precise estimate of the correction to the T dependence of $\mathrm{Im}\Sigma^{(M)}$ one should analyze the contribution from other skeleton diagrams. This analysis is given in Sec. III.

In the conclusion of this subsection we prove that S_0 is indeed the leading term in $\mathrm{Im}\Sigma^{(2)}$ for $\omega, T \ll \omega_D$ in the case of the acoustic phonon. The term S_3 is proportional to ω^2/E_F at low frequencies and can be omitted in the comparison to $S_0 \sim (\omega_D/E_F)|\omega|$. The main difference between S_0 and $S_{1,2}$ is that in the latter two additional improper integrations over ω', ω'' are present (see the Appendix). In these integrals, the frequencies ω', ω'' are not of the order of $\sim \omega_D$ and corresponding momenta are far from the Fermi surface. The thermal factors in $S_{1,2}$ introduce the restriction that at least one of the phonon frequencies has to be smaller than $|\omega|$ at $T = 0$. Therefore, in the case of the acoustic phonon, one of the momenta $\mathbf{p_1}$, $\mathbf{p_1'}$ is near $\mathbf{p}$. Let us take $\mathbf{p_1}$ to be near $\mathbf{p}$. Due to the momentum conservation momenta $\mathbf{p'}$ and $\mathbf{p_1'}$ are approximately equal. The phonon momentum $\mathbf{q_2}$ can be substituted by the momentum on the Fermi surface, Fig. 4(c). [Case 1 in Fig. 4(c) corresponds to the processes contributing to S_0 and case 2 describes the processes contributing to $S_{1,2}$.] This implies that the same function appears in the integrands of the expressions which give S_0, S_1, and S_2, except that in the case of S_0 it is multiplied by two δ functions, while in the case of $S_{1,2}$ it is multiplied by $1/(\omega' \pm \Omega_2)(\omega'' \pm \Omega_2)$. If Ω_2 differs from zero, the smallness of $S_{1,2}$ compared to S_0 at low ω and T is obvious. If $\Omega_2 \simeq 0$, the additional integra-

tion over phonon frequency makes $S_{1,2}$ small compared to S_0.

It should be noted that in 2D the correction to the imaginary part of the self-energy from $\mathrm{Im}\Sigma^{(2)}$ has a sign opposite to $\mathrm{Im}\Sigma^{(M)}$ and the two do not compensate each other near $\omega = 0$. In the case when self-energy is computed with the dressed lines the correct sign of $\mathrm{Im}\Sigma(\epsilon_p, \omega + i0^+)$ is presumably restored by contribution from other skeleton diagrams.[17]

III. CONTRIBUTION FROM $(N+1)$-ORDER DIAGRAMS TO SELF-ENERGY

Let us discuss corrections from the higher-order diagrams. Vertex Γ can be written as an infinite sum of the skeleton diagrams with dressed lines and vertices Γ.[18] We start from the skeleton diagrams for self-energy with bare vertices g instead of Γ for $(N+1)$-order diagram ($N > 1$). Each diagram with $N+1$ phonon lines has $2N+1$ electron lines and $N+1$ integrations over the electron momenta in 2D. After analytical continuation and after taking the imaginary part, the minimum number of the imaginary parts of the phonon and electron propagators is $N+2$ and the maximum number of the real parts is $2N$. The number of real parts of various propagators is important because it is equal to the number of improper integrations in $\mathrm{Im}\Sigma^{(N+1)}$ (compared to $\mathrm{Im}\Sigma^{(2)}$). We select two classes of skeleton diagrams. In one class we have diagrams, like the first diagram in Fig. 1(b), which are characterized by momentum conservation $\mathbf{q} = \mathbf{p}' - \mathbf{p} = \mathbf{p}'_1 - \mathbf{p}_1 = \cdots = \mathbf{p}'_N - \mathbf{p}_N$. In the second class we have diagrams, like the remaining two in Fig. 1(b), which are characterized by momentum conservation $\mathbf{Q} = \mathbf{p} + \mathbf{p}' = \mathbf{p}_1 + \mathbf{p}'_1 = \cdots = \mathbf{p}_N + \mathbf{p}'_N$. One can estimate the order of magnitude of a skeleton diagram from either one of these two classes in 2D. As before, the integration over momenta $\mathbf{p}', \mathbf{p}'_1, \ldots, \mathbf{p}'_N$ is replaced by the integration over the energy variables $\epsilon_{p_1}, \ldots, \epsilon_{p_N}, \epsilon_{p'}, \epsilon_{p'_1}, \ldots, \epsilon_{p'_N}$ and over $Q = |\mathbf{Q}|$ (or $q = |\mathbf{q}|$). At fixed Q (or q) a point $(\epsilon_{p_1}, \ldots, \epsilon_{p_N}, \epsilon_{p'}, \epsilon_{p'_1}, \ldots, \epsilon_{p'_N})$ corresponds to 2^{N+1} points in the momentum spaces. The one-to-one correspondence could be preserved by partitioning the momentum space in suitably chosen regions. Next we introduce the generalization of $B^{(2)}$ given by Eq. (6). In the Cooperon channel ($\mathbf{Q}$ conservation), for example, the function $B^{(N+1)}$ is defined by

$$B^{(N+1)}(\epsilon_p, \omega; \omega', \ldots, \omega^{(2N+1)}; \Omega_1 \cdots \Omega_N) = \frac{1}{E_F^N} \int_{-\infty}^{\mu} d\epsilon_{p_1} A(\epsilon_{p_1}, \omega') \cdots \int_{-\infty}^{\mu} d\epsilon_{p'_N} A(\epsilon_{p'_N}, \omega^{(2N+1)}) \frac{\theta(Q_M - Q_m)}{\pi^{N+1}} \int_{Q_m}^{Q_M} \frac{(p_F)^{2N} 2Q dQ}{X(Qpp')X(Qp_1p'_1)\cdots X(Qp_Np'_N)} \times \frac{1}{2^N} \sum_{\beta} B(q_1^{\beta}, \Omega_1) \cdots B(q_N^{\beta}, \Omega_N) . \tag{18}$$

Here the summation over β corresponds to the summation over the above-mentioned regions in the momentum space. The limits of the integration over Q are now $Q_m = \max(|p' - p|, |p'_1 - p_1|, \ldots, |p'_N - p_N|)$ and $Q_M = \min(p + p', p_1 + p'_1, \ldots, p_N + p'_N)$. The frequencies in the electron spectral weights are taken according to the energy conservation in the Cooperon channel. $B^{(N+1)}$ for a diagram with momentum conservation connected to $\mathbf{q}$ can be obtained from (18) by replacing Q with q and by using the appropriate dependencies of q_i^{β} on energies $\epsilon_{p_{i'}}$. To estimate $B^{(N+1)}$ one can substitute the phonon spectral weights $B(q_i^{\beta}, \Omega_i)$ by the average value $B_{\mathrm{av}}(\Omega_i)$. The integration over the phonon frequencies $\Omega_1, \ldots, \Omega_N$ gives the order of magnitude of the diagram under consideration. Taking the electron spectral weights for bare lines one can find the geometrical singularities of the type

$$I^{(N+1)} \simeq \int_0^{(2p_F)^2} \frac{(p_F)^{2N} dQ^2}{\{\sqrt{Q^2[(2p_F)^2 - Q^2]}\}^{N+1}} \tag{19}$$

in the expression (18), if all momenta are on the Fermi surface. These singularities are eliminated by taking the dressed electron lines, in which case the spectral weights have the Lorentzian form

$$A(\epsilon_p, \omega) = \frac{1}{\pi} \frac{(2\tau)^{-1}}{(\omega - \epsilon_p)^2 + (2\tau)^{-2}} , \tag{20}$$

where $(2\tau)^{-1}$ is the damping. Then, formulas analogous to Eq. (14) produce a result with geometrical singularities removed. Assuming a constant damping $1/\tau \ll E_F$ one finds $I^{(N+1)} \sim (E_F\tau)^{N-1}$. Taking $\tau^{-1} \simeq \pi\lambda\Omega_{\mathrm{ph}}$ (or $\tau^{-1} \simeq 2\pi\lambda T$ at high temperatures $T \sim \Omega_{\mathrm{ph}}$) the order of $\int_0^{\infty} d\Omega_1 \cdots \int_0^{\infty} d\Omega_N B^{(N+1)}$ can be estimated as $\sim \lambda^N A_N \Omega_{\mathrm{ph}}/E_F$ when variables $\epsilon_p, \omega, \omega', \ldots, \omega^{(2N+1)}$ are $\sim \Omega_{\mathrm{ph}}$, and to be smaller otherwise. Above we have found that $\mathrm{Im}\Sigma^{(2)}/\mathrm{Im}\Sigma^{(M)}$ increases linearly with temperature. Now, it is easy to check that when $\Omega_{\mathrm{ph}} \ll T \ll E_F$ the ratio $\mathrm{Im}\Sigma^{(N+1)}/\mathrm{Im}\Sigma^{(M)}$, where $\Sigma^{(N+1)}$ is the contribution of a skeleton diagram from one of the above-mentioned classes, increases with temperature as T^{δ} with $\delta \leq 1$. The Bose thermal factors for $(N+1)$-phonon lines could give the power of T which is at most $N+1$. Since $I^{(N+1)} \simeq (E_F\tau)^{N-1}$ with $\tau^{-1} \sim T$, $\mathrm{Im}\Sigma^{(N+1)}/\mathrm{Im}\Sigma^{(M)} \sim T/E_F$.

We have substituted the vertices Γ by g in the $(N+1)$-order skeleton diagram. The difference between Γ and g is of the order of Ω_{ph}/E_F in the Migdal approximation. Due to the prefactor E_F^{-N} which appears after transforming the summation over momenta $\mathbf{p}', \mathbf{p}'_1, \ldots, \mathbf{p}'_N$ to integration over the energy variables, the resulting error in $\Sigma^{(N+1)}$ is $o(\Omega_{\mathrm{ph}}/E_F)$ if Γ does not have a singularity. Singularity in Γ would lead to violation of Migdal's theorem. In Sec. VI we will show that when Γ is calcu-

lated with bare lines, the singularities appear in 2D, but dressing the bare lines with self-energy restores Migdal's theorem except in the vicinity of special points.

The interesting feature of integral (18) is that the strongest singularity is present, as in the case of $\Sigma^{(2)}$, near the line $\omega = \epsilon_p$. This is a direct consequence of the 2D-nature of the problem where all electron momenta are in the same plane. This brings a qualitative difference between the electron-phonon problem in 2D and 3D, especially with increasing $\Omega_{\rm ph}/E_F$. It was conjectured by Holstein[19] that in 3D $(N+1)$st-order diagram is of the order $(\Omega_{\rm ph}/E_F)^N$. In 2D we get for any $(N+1)$st-order diagram from the two classes described above the estimate $A_N\Omega_{\rm ph}/E_F$, where A_N is a combinatorical factor.

From the previous discussion it is clear that geometrical singularities play an extremely important role in the electron-phonon problem in 2D. The question is whether the shape of the Fermi surface influences these geometrical singularities in 2D. We would like to discuss our result for $\Sigma^{(2)}$ in the case of the electron spectrum for a nested Fermi surface, $\epsilon_{\mathbf{k}} = -2t_{||}[\cos(k_x a) + \cos(k_y a)]$, where $\mathbf{k}$ is in the first Brillouin zone. The $\mathrm{Im}\Sigma^{(2)}(\epsilon_{\mathbf{k}}, \omega)$ has the singularities too. For example, if $\mathbf{k} = (0, \pi/a)$ we can take the variable $Q_n = [\cos(Q_x a) + \cos(Q_y a)]/2$ as independent from the energy variables. Here, $\mathbf{Q} = (Q_x, Q_y)$ is the total momentum. The Jacobian for transition from integrations over momenta $dk'_x dk'_y dk'_{1x} dk'_{1y}$ to the integrations over the energy variables and over Q_n, $|J(\epsilon_{k_1}\epsilon_{k'}\epsilon_{k'_1}Q_n)|^{-1} d\epsilon_{k_1} d\epsilon_{k'} d\epsilon_{k'_1} dQ_n$, cannot be written in the analytical form for the general case. It is possible to find the Jacobian at $\epsilon_{k_1} = \epsilon_{k'_1} = 0$ and $\epsilon_{k'} = \epsilon$. It is

$$|J| = 4t_{||}|\epsilon| \frac{\sin X^{(+)} \sin X^{(-)} (\sin X^{(+)} - \sin X^{(-)})^2}{\epsilon^2 + 4t_{||}^2 (\sin X^{(+)} - \sin X^{(-)})^2}, \tag{21}$$

where $\sin X^{(\pm)} = \sqrt{1 - (Q_n \pm \epsilon/4t_{||})^2}$. For $\epsilon \approx 0$, which corresponds to the case when all momenta are located near the Fermi surface, the singularity in the Jacobian is stronger than logarithmic if $Q_n = 0$ or ± 1. These cases are shown in Figs. 4(d) and 4(e). The analogy with an isotropical cases is quite clear. One can conclude that 2D singularities will appear for any shape of the Fermi surface. Additional analysis of Migdal's theorem must be carried out in the case of a nested Fermi surface because the geometrical singularities in higher-order diagrams around several special points are stronger than those obtained for the isotropic case.

IV. THE BEHAVIOR OF SELF-ENERGY AT HIGH ω AND T

To estimate the imaginary part of the self-energy at large ω and ϵ_p the following should be mentioned. The $(N+1)$-order diagram for the self-energy has an overall prefactor of the order of $\sim (\Omega_{\rm ph}/E_F)^N$ [Eq. (18)]. This prefactor does not depend on the frequency range. Therefore, one has to study the correction to the Migdal approximation even in the first-order diagram. The imaginary part of $\Sigma^{(1)}$ can be written in the general case as

$$\mathrm{Im}\Sigma^{(1)}(\epsilon_p, \omega) = -\frac{1}{2} \sum_{\alpha_1 = \pm 1} \int_0^\infty d\Omega \left(\coth \frac{\Omega}{2T} - \alpha_1 \tanh \frac{\omega + \alpha_1 \Omega}{2T} \right) \times \int_{-\infty}^{\mu} d\epsilon_{p'} A(\epsilon_{p'}, \omega + \alpha_1 \Omega) \int_{|p-p'|}^{\min(p+p', q_0)} \frac{2q dq}{X(qpp')} B(q, \Omega). \tag{22}$$

q_0 is the cutoff for phonon momenta. Expression (2) for $\mathrm{Im}\Sigma^{(M)}$ has been obtained from Eq. (22) by taking $p, p' \sim p_F$ and by performing the integration over $\epsilon_{p'}$ in the infinite limits. Our estimation is based on the assumption that at large Ω the phonon spectral weight does not depend critically on q. First, we restrict ourselves to the case $T = 0$ and $\omega > \Omega_{\rm max}$, where $\Omega_{\rm max}$ is the maximum phonon frequency. $\mathrm{Im}\Sigma^{(M)}$ does not depend on ϵ_p. In the first step we take the spectral weights calculated within the Migdal approximation. To perform the integration over $\epsilon_{p'}$, one can exchange the order of integration in Eq. (22). After using formula (15) one gets

$$\int_{\epsilon_{p+q}}^{\epsilon_{|p-q|}} \frac{d\epsilon_{p'}}{X(qpp')} A(\epsilon_{p'}, \omega) = \mathrm{Re} \frac{1}{X[qpp(\epsilon)]}, \tag{23}$$

where $\epsilon = \omega - \Sigma^{(M)}(\omega) = Z(\omega)\omega$, with $Z(\omega)$ the renormalization parameter.[20] Formula (23) is not obtained by the residue theorem because of the finite limits of integration, but it is a direct consequence of (15). All the square roots are with positive real parts. The phonon spectral weight of a Lorentzian form and $q_0 = 2p_F$ are used in the calculations shown in Fig. 5. The main feature of the model is a decrease of the imaginary part of self-energy at high frequencies and for large electron energies. Figure 6 illustrates that with increasing $\Omega_{\rm ph}/E_F$ one cannot neglect the ϵ_p dependence on the scale of ω about several times of $\Omega_{\rm ph}$. When ω or ϵ_p are near the top of the band the decrease of $\mathrm{Im}\Sigma^{(1)}$ is fast due to a decrease in the number of the electron states near the band edge. If the sum of the electron momenta becomes larger than q_0, $\mathrm{Im}\Sigma(\epsilon_p, \omega)$ decreases because of the reduced phase space. The ϵ_p dependence of the self-energy is mainly coming from these two mechanisms. The imaginary part of the self-energy is not symmetric with respect to ω due to dependence on ϵ_p. The presence of damping in ϵ as the argument of $X[qpp(\epsilon)]$ in Eq. (23) causes the additional decrease of the imaginary part of self-energy. The interesting feature of $\Sigma^{(1)}$ is the behavior at high temperatures. To study this behavior we have plotted $\mathrm{Im}\Sigma^{(1)}(\epsilon_p, \omega)$ at $\epsilon_p = \omega = 0$ for finite temperatures. In the Migdal approximation this value reaches the limit $\pi\lambda T$ (Fig. 7). At high T, increasing the ratio $\Omega_{\rm ph}/E_F$ can cause the ef-

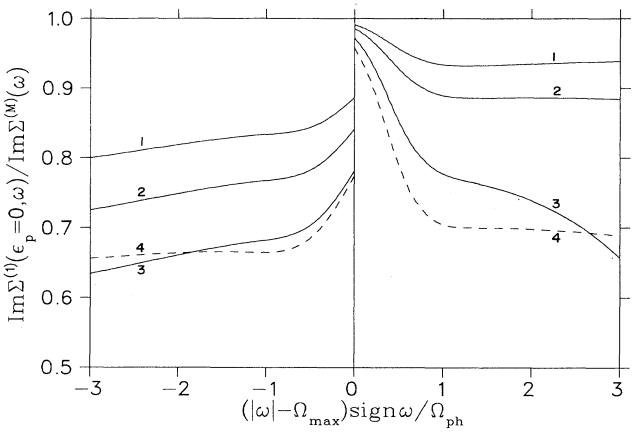

FIG. 5. The imaginary part of the self-energy at high frequencies ($T = 0$). The curves are plotted for $|\omega| > \Omega_{\max}$, $\Omega_{\max} = 1.6\Omega_{\mathrm{ph}}$. The electron spectral weights are calculated within the Migdal approximation. The solid line is for $\lambda = 1$, the dashed line is for $\lambda = 3$. Curve 1 is for $\Omega_{\mathrm{ph}} = 0.05E_F$, curve 2 is for $\Omega_{\mathrm{ph}} = 0.1E_F$, curve 3 is for $\Omega_{\mathrm{ph}} = 0.2E_F$, curve 4 is for $\Omega_{\mathrm{ph}} = 0.1E_F$.

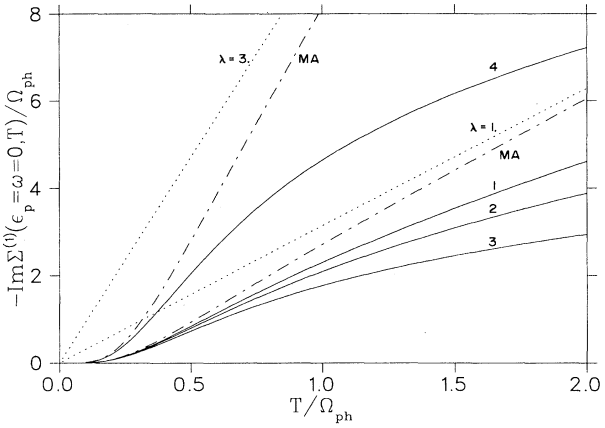

FIG. 7. The imaginary part of the self-energy at high temperatures. The dotted lines are given by $\pi\lambda T$ with λ=1 and 3 . The dot-dashed lines (MA) are calculated within the Migdal approximation with λ=1 and 3 . The solid lines are for $\Omega_{\mathrm{ph}} = 0.05E_F$, $\lambda = 1$ (curve 1); $\Omega_{\mathrm{ph}} = 0.1E_F$, $\lambda = 1$ (curve 2); $\Omega_{\mathrm{ph}} = 0.2E_F$, $\lambda = 1$ (curve 3); and $\Omega_{\mathrm{ph}} = 0.1E_F$, $\lambda = 3$ (curve 4).

fective decreasing of λ and deviation from the usual formula for inverse relaxation time. The higher-order corrections can only increase this deviation from the asymptotic value of $\pi\lambda T$. For example, one can find that the sign of the term which produces the maximum increase in $\mathrm{Im}\Sigma^{(2)}(\epsilon_p = \omega = 0)$ at high temperatures [the term which consists of the product $\coth(\Omega_1/2T)\coth(\Omega_2/2T)$] is opposite to $\mathrm{Im}\Sigma^{(1)}(\epsilon_p = \omega = 0)$. This should cause a larger decrease ($\sim T^2/E_F$) from the one shown in Fig. 7.

V. SOME LIMITING CASES FOR VERTEX

To complete our analysis of the electron-phonon interaction in 2D we would like to study the skeleton diagrams for vertex Γ at $T = 0$. The first diagram, $\Gamma^{(1)}$, shown in Fig. 8(a) has been studied in 3D.[10] The analysis of this diagram is the initial point for the Migdal approximation. It was pointed out that when we take the limits $\mathbf{q} \to 0$, $i\omega_\nu \to 0$, in that order, the magnitude of this di-

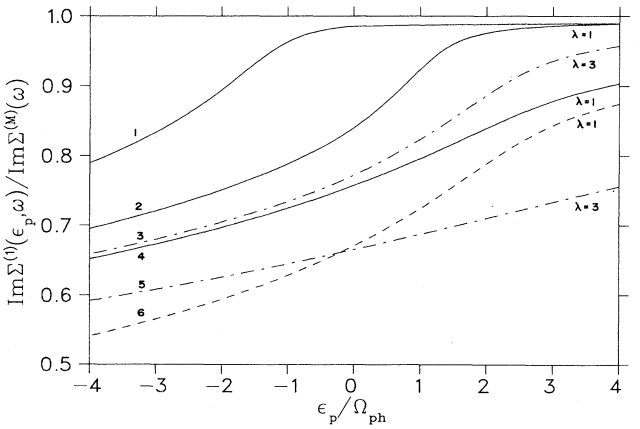

FIG. 6. The ϵ_p dependence of the imaginary part of the self-energy ($T = 0$, $\Omega_{\max} = 1.6\Omega_{\mathrm{ph}}$). Curve 1 is for $\lambda = 1$, $\omega = \Omega_{\max}$, $\Omega_{\mathrm{ph}} = 0.1E_F$; curve 2 is for $\lambda = 1$, $\omega = -\Omega_{\max}$, $\Omega_{\mathrm{ph}} = 0.1E_F$; curve 3 is for $\lambda = 3$, $\omega = -\Omega_{\max}$, $\Omega_{\mathrm{ph}} = 0.1E_F$; curve 4 is for $\lambda = 1$, $\omega = -2\Omega_{\max}$, $\Omega_{\mathrm{ph}} = 0.1E_F$; curve 5 is for $\lambda = 3$, $\omega = -2\Omega_{\max}$, $\Omega_{\mathrm{ph}} = 0.1E_F$; and curve 6 is for $\lambda = 1$, $\omega = -2\Omega_{\max}$, $\Omega_{\mathrm{ph}} = 0.2E_F$.

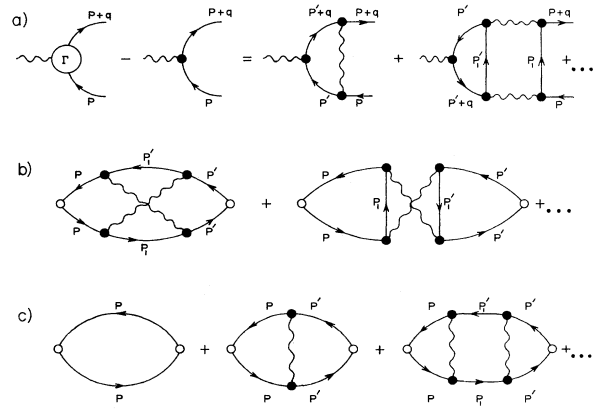

FIG. 8. Diagrams for the three-point vertex $\Gamma(\mathbf{p},\omega;\mathbf{q},\nu)$ (a) and the polarization part $\Pi(\mathbf{q},\nu)$ (b) and (c). The contribution of the first diagram in the right side of (a) is on the order of Ω_{ph}/E_F. The second diagram in the right side of (a) has the geometrical singularities in 2D [Eqs. (32) and (33)]. The diagrams with crossed phonon lines in (b) have the geometrical singularities in 2D which increase their importance near $\nu \simeq 0$.

agram is $\Omega_{\rm ph}/E_F$. Here $i\omega_\nu$ is the Matsubara frequency for the incoming phonon and $\mathbf{q}$ is its momentum. The order of the limits is important because in the reversed order $i\omega_\nu \to 0$, $\mathbf{q} \to 0$ the vertex is $O(1)$.[20,21] In 2D it is not enough to study only $\Gamma^{(1)}$ even when $\Omega_{\rm ph}/E_F$ is small. To illustrate our point we would like to compare two diagrams shown in Fig. 8(a). The calculations with bare lines for vertex corrections $\Gamma^{(1)}$ and $\Gamma^{(2)}$ give

$$\lim_{\mathbf{q}\to 0}\lim_{i\omega_\nu\to 0}\Gamma^{(1)} = N(0)^{-1}\sum_{\mathbf{p}'}\int_0^{+\infty} d\Omega B(\mathbf{p}-\mathbf{p}',\Omega)\sum_{\alpha=\pm 1}\alpha\frac{\partial}{\partial\epsilon_{p'}}\left[\frac{\delta_{\alpha,-1}-f(\epsilon_{p'})}{i\omega_n+\alpha\Omega-\epsilon_{p'}}\right], \tag{24}$$

$$\lim_{\mathbf{q}\to 0}\lim_{i\omega_\nu\to 0}\Gamma^{(2)} = N(0)^{-2}\sum_{\mathbf{p}'\mathbf{p}_1'}\int_0^{+\infty} d\Omega_1 B(\mathbf{p}-\mathbf{p}_1,\Omega_1)\int_0^{+\infty} d\Omega_2 B(\mathbf{p}-\mathbf{p}_1,\Omega_2)$$
$$\times\sum_{\alpha_1,\alpha_2=\pm 1}\frac{\alpha_1\alpha_2}{\alpha_1\Omega_1-\alpha_2\Omega_2}\frac{\partial}{\partial\epsilon_{p'}}\left[\frac{K_{\alpha_1}(\Omega_1)-K_{\alpha_2}(\Omega_2)}{i\omega_n+\epsilon_{p'}-\epsilon_{p_1}-\epsilon_{p_1'}}\right], \tag{25}$$

$$K_\alpha(\Omega) = \frac{I_1}{i\omega_n-\epsilon_{p_1}+\alpha\Omega}-\frac{I_2}{\epsilon_{p'}-\epsilon_{p_1'}-\alpha\Omega},$$

where $\mathbf{p}$ and $i\omega_n$ are, respectively, the momentum and the frequency for the incoming electron line, $\delta_{\alpha,-1}$ is the Kronecker symbol. I_1, I_2 are the factors containing various combinations of the Fermi and Bose functions. For $T=0$ they consist of the sum of the products of θ functions because of $f(\epsilon) = -N(\epsilon) = \theta(-\epsilon)$:

$$I_1 = [\delta_{\alpha,-1}-f(\epsilon_{p_1})]f(\epsilon_{p'})+[\delta_{\alpha,1}-f(\epsilon_{p_1'})]f(\epsilon_{p'}+\alpha\Omega)$$
$$+[1-f(\epsilon_{p_1})-f(\epsilon_{p_1'})]N(\epsilon_{p_1}+\epsilon_{p_1'}), \tag{26}$$
$$I_2 = [\delta_{\alpha,1}-f(\epsilon_{p_1'})][f(\epsilon_{p'})-f(\epsilon_{p_1'}+\alpha\Omega)]. \tag{27}$$

After analytical continuation $i\omega_n \to \omega + i0^+$, the limits in Eqs. (24) and (25) will be denoted as $\Gamma^{(1)}(\epsilon_p,\omega)$ and $\Gamma^{(2)}(\epsilon_p,\omega)$, respectively. We are interested in the case when the characteristic phonon frequency is much smaller than the Fermi energy and $\omega \sim \Omega_{\rm ph}$. Therefore, only the first order of $\Omega_{\rm ph}/E_F$ will be kept. The denominator under the integral in Eq. (24) is peaked near the Fermi surface. Thus, the integration over energy variable can be separated from integration over phonon momentum, assuming that the $\mathbf{q}$ dependence of $B(\mathbf{q},\Omega)$ is not significant. Taking $-\epsilon_p = p^2/2m-\mu$, as we have done in the calculations of $\Sigma^{(2)}$, one obtains

$$\Gamma^{(1)}(\epsilon_p,\omega) \approx -\frac{1}{E_F}\sum_{\mathbf{q}}\int_0^{+\infty} d\Omega B(\mathbf{q},\Omega),$$
$$\mathrm{Im}\Gamma^{(1)}(\epsilon_p,\omega) \approx 0\,. \tag{28}$$

The order of magnitude of $\Gamma^{(1)}(\epsilon_p,\omega)$ is the same in both 2D and 3D. For example, the result of the calculation of $\Gamma^{(1)}(\epsilon_p,\omega)$ with $B(\mathbf{q},\Omega)$ given by the Einstein model is $-\lambda\Omega_{\rm ph}^{(0)}/2E_F$, while for the 3D Debye model it is $-\lambda\omega_D/3E_F$ and for the 2D Debye model it is $-\lambda\omega_D/\pi E_F$. The imaginary part of the first-order vertex correction, $\Gamma^{(1)}$, is $o(\Omega_{\rm ph}/E_F)$. However, the imaginary part of $\Gamma^{(2)}(\epsilon_p,\omega)$ is $O(\Omega_{\rm ph}/E_F)$. Indeed, after substituting the phonon spectral weight by the average $B_{\rm av}(\Omega)$ and after transforming the integration variables to $\epsilon_{p'}, \epsilon_{p_1'}, \epsilon_{p_1}, Q$ we get

$$\text{(3D)}:\ N_{\rm 3D}(0)^{-2}\sum_{\mathbf{p}',\mathbf{p}_1'}\cdots = \frac{1}{E_F}\int_{-\infty}^{E_F}d\epsilon_{p'}\int_{-\infty}^{E_F}d\epsilon_{p_1'}\int_{-\infty}^{E_F}d\epsilon_{p_1}\theta(Q_M-Q_m)\int_{Q_m}^{Q_M}\frac{dQ}{2p}\cdots \tag{29}$$

and

$$\text{(2D)}:\ N(0)^{-2}\sum_{\mathbf{p}',\mathbf{p}_1'}\cdots = \frac{1}{E_F}\int_{-\infty}^{E_F}d\epsilon_{p'}\int_{-\infty}^{E_F}d\epsilon_{p_1'}\int_{-\infty}^{E_F}d\epsilon_{p_1}\frac{\theta(Q_M-Q_m)}{\pi^2}\int_{Q_m}^{Q_M}\frac{p_F^2 2QdQ}{X(Qpp')X(Qp_1p_1')}\cdots. \tag{30}$$

Here $N_{\rm 3D}(0) = mp_F/2\pi^2$ is the three-dimensional electron density of states at the Fermi level. The momenta Q_m and Q_M are the same as in Eq. (10): $Q_m = \max(|p-p'|,|p_1-p_1'|)$, $Q_M = \min(p+p',p_1+p_1')$. The imaginary part of $\Gamma^{(2)}(\epsilon_p,\omega)$ has a δ function which removes one integration, say, over ϵ_{p_1}. If the incoming momentum $\mathbf{p}$ is near the Fermi surface $p \sim p_F(\epsilon_p \sim \Omega_{\rm ph})$, the function $\theta(Q_M-Q_m)$ and the thermal factors I_1, I_2 provide a cutoff, $E_0(\sim E_F)$, for integrations over $\epsilon_{p'}, \epsilon_{p_1'}$. In 3D one can estimate the imaginary part of the second-order vertex correction for the Einstein model to be

$$\mathrm{Im}\Gamma^{(2)}(\epsilon_p,\omega) \sim -\frac{\pi}{4}\lambda^2\frac{\Omega_{\rm ph}^{(0)}}{E_F}\ln\frac{E_F+E_0}{E_F}\theta(|\omega|-\Omega_{\rm ph}^{(0)}). \tag{31}$$

This shows that in 3D $\mathrm{Im}\Gamma^{(2)} \sim O(\Omega_{\mathrm{ph}}/E_F)$ for $|\omega| > \Omega_{\mathrm{ph}}^{(0)}$, while $\mathrm{Im}\Gamma^{(1)} \sim o(\Omega_{\mathrm{ph}}/E_F)$. Let us estimate the imaginary part of the second-order vertex correction in the case of the Einstein model for 2D electron gas in the region $|\omega| < \Omega_{\mathrm{ph}}^{(0)}$. By extracting the geometrical singularities from the integral over Q in (30) and by combining them with thermal factors which keep the energies near the Fermi level, one can find the singularity in $\mathrm{Im}\Gamma^{(2)}$

$$\mathrm{Im}\Gamma^{(2)}(\epsilon_p,\omega) \sim -\frac{\lambda^2}{2\pi}\frac{\Omega_{\mathrm{ph}}^{(0)}}{4E_F}\left[\omega \ln\frac{\Omega_{\mathrm{ph}}^{(0)}+\omega}{\Omega_{\mathrm{ph}}^{(0)}-\omega} + \frac{\omega^2\Omega_{\mathrm{ph}}^{(0)}}{\Omega_{\mathrm{ph}}^{(0)2}-\omega^2}\right]\frac{1}{\omega-\epsilon_p}. \quad (32)$$

This asymptotic formula reflects the fast increase of the vertex correction $\mathrm{Im}\Gamma^{(2)}$ in the vicinity of $\omega \approx \epsilon_p$. The term $(\omega-\epsilon_p)^{-1}$ in Eq. (32) does not depend on the Einstein model, but it appears in the general case because it is connected with the two-dimensionality of the free electron gas. Indeed, one can substitute the average spectral weight $B_{\mathrm{av}}(\Omega)$ by the Eliashberg function $\alpha^2F(\Omega)$ and estimate the behavior of the imaginary part of the second-order vertex correction at low frequencies $\omega \ll \Omega_{\mathrm{ph}}$. The result is

$$\mathrm{Im}\Gamma^{(2)}(\epsilon_p,\omega) \sim -\frac{3\lambda^2}{8\pi E_F}\frac{\omega^2}{\omega-\epsilon_p}. \quad (33)$$

When $\epsilon_p \approx \omega + O(\omega^2/E_F)$, the terms with higher powers of E_F^{-1} should be taken into account. Including such terms does not change the tendency of the vertex with bare lines to increase in the vicinity of $\omega = \epsilon_p$ and to be larger than the bare vertex. It is clear that the diagram for the vertex correction with more than two phonon lines gives stronger geometrical singularities in 2D near $\omega \approx \epsilon_p$. If the damping is finite ($\sim \Omega_{\mathrm{ph}}$), the singular term $(\omega-\epsilon_p)^{-1}$ in the vertex correction $\mathrm{Im}\Gamma^{(2)}$ in Eq. (32) is replaced by a term of the order of $\Omega_{\mathrm{ph}}^{-1}$, and Migdal's result for vertex is retrieved. At low frequencies, the prefactor of the singular term decreases rapidly. One can conclude that the order of the vertex corrections in 2D calculated with dressed lines does not exceed the order of the main accuracy $\sim \Omega_{\mathrm{ph}}/E_F$ but in the vicinity of some special points the contribution from the vertex correction in 2D is much larger than in 3D.

VI. POLARIZATION PART AT q = 0

Due to the importance of the polarization part $\Pi(\mathbf{q},\nu)$ in the limit of $|\mathbf{q}| \to 0$ for transport and optical properties of the electron-phonon system, let us discuss briefly the higher-order diagrams shown in Fig. 8(b) for $\mathrm{Im}P(\nu) = \lim_{q\to 0}\mathrm{Im}\Pi(q,\nu)$ in 2D. The vicinity of $q = 0$ does not play a significant role for phonon polarization,[19] and we omit the external vertices which are denoted as open circles in Fig. 8. The diagram without phonon lines (the simple polarization bubble) and the bubble with one phonon line have the same value in 2D and 3D because of the absence of geometrical singularities in the integration over momenta. The difference appears in diagrams with two or more phonon lines. The diagrams in Fig. 8(b) involve integrations over the frequencies ω,ω',ω'' and summations over momenta $\mathbf{p},\mathbf{p}',\mathbf{p}_1'$. In the case of the polarization part $\Pi(\mathbf{q},\nu)$, the function analogous to $B^{(2)}$, Eq. (6), that appeared in the results for $\Sigma^{(2)}$, is $P^{(2)}$

$$P^{(2)}(\nu;\omega,\omega',\omega'',\omega''';\Omega_1\Omega_2) = \frac{1}{E_F}\int_{-\infty}^{\mu}d\epsilon_p\int_{-\infty}^{\mu}d\epsilon_{p_1}\int_{-\infty}^{\mu}d\epsilon_{p'}\int_{-\infty}^{\mu}d\epsilon_{p_1'} \times A(\epsilon_p,\omega)A(\epsilon_p,\omega+\nu)A(\epsilon_{p'},\omega')A(\epsilon_{p'},\omega'+\nu)A(\epsilon_{p_1},\omega'')A(\epsilon_{p_1'},\omega''') \times\frac{\theta(Q_M-Q_m)}{\pi^2}\int_{Q_m}^{Q_M}\frac{(p_F)^2 2QdQ}{X(Qp_1p_1')X(Qpp')}\frac{1}{2}\sum_{\beta}B(q_1^{\beta},\Omega_1)B(q_2^{\beta},\Omega_2). \quad (34)$$

The summation over β is the summation over $\pm$, as in Eq. (10), and over two diagrams in Fig. 8(b). In the case of $q \ll 2p_F$, the calculation of the simple bubble with bare lines gives nonzero result for $\mathrm{Im}\Pi(\mathbf{q},\nu)$ only on the scale of $\nu \sim v_F q$.[12,22] At $q = 0$ the simple bubble [Fig. 8(c)] calculated with dressed lines $G^{(M)}(\epsilon_p,\omega)$ gives $\mathrm{Im}P(\nu) \sim N(0)\nu\tau^{-1}(\nu)/[\nu^2+\tau^{-2}(\nu)]$, with $\tau^{-1}(\nu)$ related to damping.[23] The strong temperature dependence of the polarization part, especially in the region of the low frequencies, was found.[23] Including the diagrams in the ladder approximation [Fig. 8(c)] does not change this result.[24] We argue that increasing Ω_{ph}/E_F can affect temperature dependence of the polarization part in 2D. In the region of small ν, one can estimate the contribution to the polarization part from the diagrams in Fig. 8(b) to be larger than the contribution from the series of ladder diagrams in Fig. 8(c). Indeed, the products $A(\epsilon,\omega)A(\epsilon,\omega+\nu)$ in expression (34) can be substituted at small ν by the derivatives $\frac{\partial}{\partial\epsilon}A(\epsilon,\omega)$. In 2D, the derivatives with respect to the energy increase the order of geometrical singularities near $\nu = 0$ in diagrams shown in Fig. 8(b) [compare to the case of limits for vertex function Γ in Eqs.(25) and (32)]. At large ν the contribution to $\mathrm{Im}P(\nu)$ from these diagrams is small [$\sim N(0)\Omega_{\mathrm{ph}}/E_F \ln(E_F/\Omega_{\mathrm{ph}})$]. However, at high frequencies ν and/or at high temperatures T the changes are already present in the simple bubble due to the correction of the frequency and temperature dependences of

$\mathrm{Im}\Sigma(\epsilon_p,\omega)$ (see Sec IV). In future work we will study in a more quantitative way the effect of two-dimensionality and increasing Ω_{ph}/E_F on $\mathrm{Im}\Pi(\mathbf{q},\nu;T)$.

VII. CONCLUSIONS

The main difference between 2D and 3D electron gas is that in 2D all electron momenta are in the same plane. This leads to geometrical singularities in the expressions for skeleton diagrams with more than one phonon line. This result is not restricted to the case of isotropic Fermi surface. In fact, we found that in the case of a nested Fermi surface in 2D the singularities are even stronger (see Sec. III). Due to geometrical singularities the many-particle effects in 2D become important even at small ratios Ω_{ph}/E_F. For example, it is not possible to describe the electron self-energy near $\omega = T = 0$ in terms of a single phonon spectral weight, $B(\mathbf{q},\Omega)$. Indeed, we found that on the energy scale $\sim \Omega_{\mathrm{ph}}^2/E_F$ near $\omega = T = 0$ the contribution to $\mathrm{Im}\Sigma(\epsilon_p,\omega)$ from the skeleton diagram with two phonon lines in 2D is larger than Migdal's result $\mathrm{Im}\Sigma^{(M)}(\omega)$.[25]

With increasing Ω_{ph}/E_F the electron states with momenta which are farther from the Fermi surface become involved in the scattering processes and one has to use the complete spectral weight $A(\epsilon_p,\omega)$ for those states, instead of δ functions. The damping is connected with $\mathrm{Im}\Sigma(\epsilon_p,\omega)$ and it determines the scale of energies where the electron spectral weight $A(\epsilon_p,\omega)$ is peaked. This scale is $\tau^{-1} \sim \pi\lambda\Omega_{\mathrm{ph}}$. Furthermore, the damping smears the geometrical singularities in 2D in the higher-order diagrams. Thus, the damping, which is related to the nature of the boson exchange between electrons, plays a key role in 2D.

Our results do not depend critically on the concrete form of the boson spectral weight $B(q,\Omega)$ as long as it extends over the frequency range restricted by Ω_B and over the momentum range restricted by $q_0 \sim 2p_F$. In the case when electrons interact via exchange of phonons and some additional bosonic excitations (e.g., spin fluctuations) the relevant parameter is $\int_0^\infty d\Omega\left[\alpha^2F(\Omega) + \sum_{\mathbf{q}} B(\mathbf{q},\Omega)\right]/E_F$. For a more precise estimate of the accuracy of calculations which use only the first-order skeleton diagram it is necessary to study in more detail the concrete connection between the three-point vertex and the four-point vertex (the Bethe-Salpeter equation for vertex). Nevertheless, it is clear that increasing Ω_B/E_F enhances the relative correction of the result obtained within the Migdal approximation and it expands the region near $\omega = T = 0$, where the corrections to the imaginary part of the self-energy are larger than $\mathrm{Im}\Sigma^{(M)}(\omega)$. At small ω the hopping in the direction perpendicular to the plane cannot be ignored. The magnitude of t/E_F, where t is the hopping matrix element, is critical, but when $t \lesssim \Omega_B^2/E_F$ the geometrical singularities still play the dominant role. Therefore, if $\Omega_B^2/E_F \sim 10$ meV, the results obtained by means of the usual treatment through the first-order diagram cannot be applied in the frequency region ~ 10 meV at low temperatures in the case of two-dimensional electron spectrum.

The asymptotic formula $\lambda(\Omega_{\mathrm{ph}} + aT)E_F^{-1}\ln(E_F/\Omega_{\mathrm{ph}})$ which gives the accuracy of the Migdal-Eliashberg approach can be applied for small values of the ratio Ω_{ph}/E_F. When Ω_{ph}/E_F is larger than 0.1–0.2 and $\lambda \gtrsim 1$, 2D electron self-energy has to be analyzed beyond the Migdal approximation in the region of frequencies and temperatures $\sim 0.2 - 0.3\Omega_{\mathrm{ph}}$. To obtain the true behavior of the imaginary part of the self-energy in this region it is necessary to take into account the higher-order corrections because in 2D the $(N+1)$st-order diagram is $\sim A_N\Omega_{\mathrm{ph}}/E_F$, and not $\sim A_N(\Omega_{\mathrm{ph}}/E_F)^N$. The consequence of our analysis is that restrictions on the range of values ω, ϵ_p, T, and $\lambda\Omega_{\mathrm{ph}}/E_F$ exist for the Migdal-Eliashberg approach. If the ratio Ω_{ph}/E_F is not negligibly small the extrapolation of the usual formulas based on the first-order diagram beyond a restricted region (see Secs. II and IV) can lead to an underestimation of the importance of the electron-phonon interaction in quasi-two-dimensional systems.

ACKNOWLEDGMENTS

The authors are thankful to Prof. G. M. Eliashberg for his interest in the results of this paper. This research was supported by the Natural Sciences and Engineering Research Council of Canada.

APPENDIX

The analytical continuation of Eq. (3) is unique if $\mathrm{Im}\Sigma(\epsilon_p,z)$ is bounded at all $\mathrm{Im}z > 0$.[16] According to the classification of terms $S_i, i = 1,2$ in Eq. (4) one can get

$$
\begin{aligned}
S_1(\epsilon_p,\omega) = -\frac{\pi}{4}\int_0^\infty d\Omega_1 \int_0^\infty d\Omega_2 \int_{-\infty}^\infty \frac{d\omega'}{\omega'-\omega}\int_{-\infty}^\infty \frac{d\omega''}{\omega''-\omega}\sum_{\alpha_1,\alpha_2=\pm 1}
&\times\left\{2\left(\coth\frac{\Omega_1}{2T} - \alpha_1\tanh\frac{\omega+\alpha_1\Omega_1}{2T}\right)\coth\frac{\Omega_2}{2T}\right.\\
&\times B^{(2)}(\epsilon_p,\omega;\omega+\alpha_1\Omega_1,\omega'+\alpha_1\Omega_1+\alpha_2\Omega_2,\omega''+\alpha_2\Omega_2;\Omega_1\Omega_2)\\
&+\left[\coth\frac{\Omega_1}{2T}\coth\frac{\Omega_2}{2T} - \frac{1}{2}\left(\coth\frac{\Omega_1}{2T}\alpha_2\tanh\frac{\omega+\alpha_2\Omega_2}{2T} + \alpha_1\tanh\frac{\omega+\alpha_1\Omega_1}{2T}\coth\frac{\Omega_2}{2T}\right)\right.\\
&-\frac{1}{2}\alpha_1\alpha_2\left(\alpha_1\coth\frac{\Omega_1}{2T} - \tanh\frac{\omega+\alpha_1\Omega_1}{2T} + \alpha_2\coth\frac{\Omega_2}{2T} - \tanh\frac{\omega+\alpha_2\Omega_2}{2T}\right)\\
&\left.\left.\times\tanh\frac{\omega+\alpha_1\Omega_1+\alpha_2\Omega_2}{2T}\right]B^{(2)}(\epsilon_p,\omega;\omega'+\alpha_1\Omega_1,\omega+\alpha_1\Omega_1+\alpha_2\Omega_2,\omega''+\alpha_2\Omega_2;\Omega_1\Omega_2)\right\}
\end{aligned}
$$

and

$$S_2(\epsilon_p,\omega) = -\frac{\pi}{4}\int_0^\infty d\Omega_1 \int_0^\infty d\Omega_2 \int_{-\infty}^\infty \frac{2\Omega_1 d\omega'}{(\omega'-\omega)^2-\Omega_1^2}\int_{-\infty}^\infty \frac{d\omega''}{\omega''-\omega}\sum_{\alpha_2=\pm 1}$$
$$\times\left\{2\tanh\frac{\omega'}{2T}\left(\coth\frac{\Omega_2}{2T}-\alpha_2\tanh\frac{\omega+\alpha_2\Omega_2}{2T}\right)B^{(2)}(\epsilon_p,\omega;\omega',\omega''+\alpha_2\Omega_2,\omega+\alpha_2\Omega_2;\Omega_1\Omega_2)\right.$$
$$+\left[\tanh\frac{\omega'+\alpha_2\Omega_2}{2T}\left(\coth\frac{\Omega_2}{2T}-\alpha_2\tanh\frac{\omega+\alpha_2\Omega_2}{2T}\right)+\alpha_2\tanh\frac{\omega'+\alpha_2\Omega_2}{2T}\right.$$
$$\times\left(\coth\frac{\omega'-\omega}{2T}-\tanh\frac{\omega'}{2T}\right)+\tanh\frac{\omega'}{2T}\coth\frac{\Omega_2}{2T}-\coth\frac{\omega'-\omega}{2T}\alpha_2\tanh\frac{\omega+\alpha_2\Omega_2}{2T}\Big]$$
$$\left.\times B^{(2)}(\epsilon_p,\omega;\omega'+\omega''-\omega,\omega'+\alpha_2\Omega_2,\omega+\alpha_2\Omega_2;\Omega_1\Omega_2)\right\},$$

where the function $B^{(2)}$ is defined in Eq. (6). The symmetry of the diagram $\Sigma^{(2)}$ in respect to the exchange between the electron line with momentum p_1 and the phonon line with momentum q_1 from one side and the electron line with momentum p_1' and the phonon line with momentum q_2 from another side is used to compact the expression for S_1 and S_2. The term S_3 is

$$S_3(\epsilon_p,\omega) = \frac{\pi}{4}\int_0^\infty d\Omega_1 \int_0^\infty d\Omega_2 \int_{-\infty}^\infty \frac{2\Omega_1 d\omega'}{(\omega'-\omega)^2-\Omega_1^2}\int_{-\infty}^\infty \frac{2\Omega_2 d\omega''}{(\omega''-\omega)^2-\Omega_2^2}$$
$$\times\left[\frac{1}{2}\left(\coth\frac{\omega'-\omega}{2T}-\tanh\frac{\omega'}{2T}+\coth\frac{\omega''-\omega}{2T}-\tanh\frac{\omega''}{2T}\right)\tanh\frac{\omega'+\omega''-\omega}{2T}\right.$$
$$\left.-\frac{1}{2}\left(\tanh\frac{\omega'}{2T}\coth\frac{\omega''-\omega}{2T}+\coth\frac{\omega'-\omega}{2T}\tanh\frac{\omega''}{2T}\right)+\tanh\frac{\omega'}{2T}\tanh\frac{\omega''}{2T}\right]$$
$$\times B^{(2)}(\epsilon_p,\omega;\omega',\omega'+\omega''-\omega,\omega'';\Omega_1\Omega_2)\,.$$

The connection of thermal factors in the expressions for S_i, $i=1,2,3$, with Bose and Fermi functions is due to

$$\coth\frac{\Omega}{2T} = 2N(\Omega)+1$$

and

$$\tanh\frac{\omega}{2T} = 1-2f(\omega)\,.$$

[1] C.G. Olson, R. Liu, D.W. Lynch, R.S. List, A.J. Arko, B.W. Veal, Y.C. Chang, P.Z. Jiang, and A.P. Paulikas, Phys. Rev. B **42**, 381 (1990).

[2] T. Takahashi, Jpn. J. Appl. Phys. **7** 141 (1992).

[3] B. Renker, F. Gompf, E. Gering, N. Nücker, D. Ewert, W. Reichardt, and H. Rietschel, Z. Phys. B **67**, 15 (1987).

[4] T. Hasegawa, H. Ikuta, and K. Kitazawa, in *Physical Properties of High Temperature Superconductors III*, edited by D.M. Ginsberg (World Scientific, Singapore, 1992).

[5] G.M. Eliashberg, Zh. Eksp. Teor. Fiz. **38**, 966 (1960) [Sov. Phys. JETP **11**, 696 (1960)].

[6] D.B. Tanner and T. Timusk, in *Physical Properties of High Temperature Superconductors III*, edited by D.M. Ginsberg (World Scientific, Singapore, 1992).

[7] C. Thomsen, in *Light Scattering in Solids VI*, edited by M. Cardona and G. Güntherodt (Springer, Heidelberg, 1991), p. 285.

[8] S. Uchida, Physica C **185-189**, 28 (1991).

[9] R.E. Cohen, H. Krakauer, and W.E. Pickett, in *High-Temperature Superconductivity*, edited by J. Ashkenazi, S.E. Barnes, F. Zuo, G.C. Vezzoli, and B.M. Klein (Plenum, New York, 1991), p. 7.

[10] A.B. Migdal, Zh. Eksp. Teor. Fiz. **34**, 1438 (1958) [Sov. Phys. JETP **7**, 996 (1958)].

[11] G.M. Eliashberg, in *High Temperature Superconductivity from Russia*, edited by A.I. Larkin and N.V. Zavaritsky (World Scientific, Singapore, 1989).

[12] A.A. Abrikosov, L.P. Gor'kov, and I.Ye. Dzyaloshinsky, *Quantum Field Theoretical Methods in Statistical Physics* (Pergamon, New York, 1965).

[13] The polynomials (9) give the Jacobian for transition from momentum variables to the energy variables in the higher-order diagram. In the case of $\Sigma^{(1)}(\epsilon_p,\omega)$ the change of integration variables from angle to phonon momentum $|\mathbf{q}|$ gives the factor $1/X(qpp')$. At p and $p' \sim p_F$ the above mentioned result for the Debye model in 2D is that $\alpha^2F(\Omega)$ is proportional to Ω and the square-root singularity due to $X(qp_Fp_F) = q[(2p_F)^2-q^2]^{1/2}$ appears.

[14] S. Fujimoto, J. Phys. Soc. Jpn. **59**, 2316 (1990).

[15] E.I. Kats, Zh. Eksp. Teor. Fiz. **56**, 1675 (1969) [Sov. Phys. JETP **29**, 897 (1969)].

[16] P.B. Allen and B. Mitrović, in *Solid State Physics*, edited by H. Ehrenreich, F. Seitz, and D. Turnbull (Academic, New York, 1992), Vol. 37.

[17] Note that when $\Sigma^{(2)}$ is calculated with bare lines the contribution from the other two nonskeleton diagrams with two phonon lines will restore the correct sign of $\mathrm{Im}\Sigma(\epsilon_p,\omega+i0^+)$ calculated up to the second order in phonon propagators.

[18] A.L. Fetter and J.D. Walecka, *Quantum Theory of Many Particle Systems* (McGraw-Hill, New York, 1971).

[19]T. Holstein, Ann. Phys. (N.Y.) **29**, 410 (1964).
[20]D.J. Scalapino, in *Superconductivity*, edited by R.D. Parks (Dekker, New York, 1969), Vol. 1, Chap. 10, p. 449.
[21]S. Engelsberg and J.R. Schrieffer, Phys. Rev. **134**, 993 (1963).
[22]A.A. Abrikosov, L.A. Fal'kovsky, Zh. Eksp. Teor. Fiz. **40**, 269 (1961) [Sov. Phys. JETP **13**, 179 (1961)].
[23]V.N. Kostur and G.M. Eliashberg, Pis'ma Zh. Eksp. Teor. Fiz. **53**, 373 (1991) [JETP Lett. **53**, 391 (1991)].
[24]V.N. Kostur, Z. Phys. B **89**, 149 (1992).
[25]We also argued, on general grounds, that in this energy region the contribution of skeleton diagrams with three or more phonon lines cannot be ignored. It is clear that the higher-order diagrams do not compensate each other trivially because of a different type of geometrical singularities for Nth- and $(N+1)$st-order diagrams [see Eq. (19)].